ESC European Society of Cardiology

European Heart Journal (2023) **44**, 1748–1760
https://doi.org/10.1093/eurheartj/ehad114

TRANSLATIONAL RESEARCH
Ischaemic heart disease

Intrapericardial long non-coding RNA–*Tcf21* antisense RNA inducing demethylation administration promotes cardiac repair

Dashuai Zhu [1,2], Shuo Liu [1,2], Ke Huang[1,2], Junlang Li[1,2], Xuan Mei[1,2], Zhenhua Li[1,2], and Ke Cheng [1,2]*

[1]Joint Department of Biomedical Engineering, North Carolina State University & University of North Carolina at Chapel Hill, 1001 William Moore Drive, Raleigh, NC 27607, USA; and [2]Department of Molecular Biomedical Sciences, North Carolina State University, 1001 William Moore Drive, Raleigh, NC 27607, USA

Received 21 April 2022; revised 1 February 2023; accepted 16 February 2023; online publish-ahead-of-print 14 March 2023

See the editorial comment for this article 'Lnc-ing epicardium-derived cells to cardiac remodelling: lncRNA-TARID as a novel antifibrotic option', by X. Wu *et al.*, https://doi.org/10.1093/eurheartj/ehad058.

Abstract

Aims Epicardium and epicardium-derived cells are critical players in myocardial fibrosis. Mesenchymal stem cell–derived extracellular vesicles (EVs) have been studied for cardiac repair to improve cardiac remodelling, but the actual mechanisms remain elusive. The aim of this study is to investigate the mechanisms of EV therapy for improving cardiac remodelling and develop a promising treatment addressing myocardial fibrosis.

Methods and results Extracellular vesicles were intrapericardially injected for mice myocardial infarction treatment. RNA-seq, *in vitro* gain- and loss-of-function experiments, and *in vivo* studies were performed to identify targets that can be used for myocardial fibrosis treatment. Afterward, a lipid nanoparticle–based long non-coding RNA (lncRNA) therapy was prepared for mouse and porcine models of myocardial infarction treatment. Intrapericardial injection of EVs improved adverse myocardial remodelling in mouse models of myocardial infarction. Mechanistically, *Tcf21* was identified as a potential target to improve cardiac remodelling. Loss of *Tcf21* function in epicardium-derived cells caused increased myofibroblast differentiation, whereas forced *Tcf21* overexpression suppressed transforming growth factor-β signalling and myofibroblast differentiation. LncRNA–*Tcf21* antisense RNA inducing demethylation (TARID) that enriched in EVs was identified to up-regulate *Tcf21* expression. Formulated lncRNA–TARID-laden lipid nanoparticles up-regulated *Tcf21* expression in epicardium-derived cells and improved cardiac function and histology in mouse and porcine models of myocardial infarction.

Conclusion This study identified *Tcf21* as a critical target for improving cardiac fibrosis. Up-regulating *Tcf21* by using lncRNA–TARID-laden lipid nanoparticles could be a promising way to treat myocardial fibrosis. This study established novel mechanisms underlying EV therapy for improving adverse remodelling and proposed a lncRNA therapy for cardiac fibrosis.

* Corresponding author. Tel: +919 513 6157, Fax: +919 513 7301, Email: ke_cheng@ncsu.edu

Structured Graphical Abstract

Key Question

What are the functional ingredients, e.g. noncoding RNAs, in stem cell-derived extracellular vesicles (EVs) and how can this be harnessed to create "super" EVs and RNA therapies to treat cardiac fibrosis?

Key Finding

Tcf21 played a critical role in determining the fate of epicardium-derived cells. Lipid nanoparticle (LNP) based lncRNA-TARID (LNP-TARID) therapy upregulated *Tcf21* and improved cardiac remodeling and functions in mouse and pig models of myocardial infarction.

Take Home Message

This study develops a lncRNA therapy to upregulate *Tcf21* for myocardial fibrosis treatment.

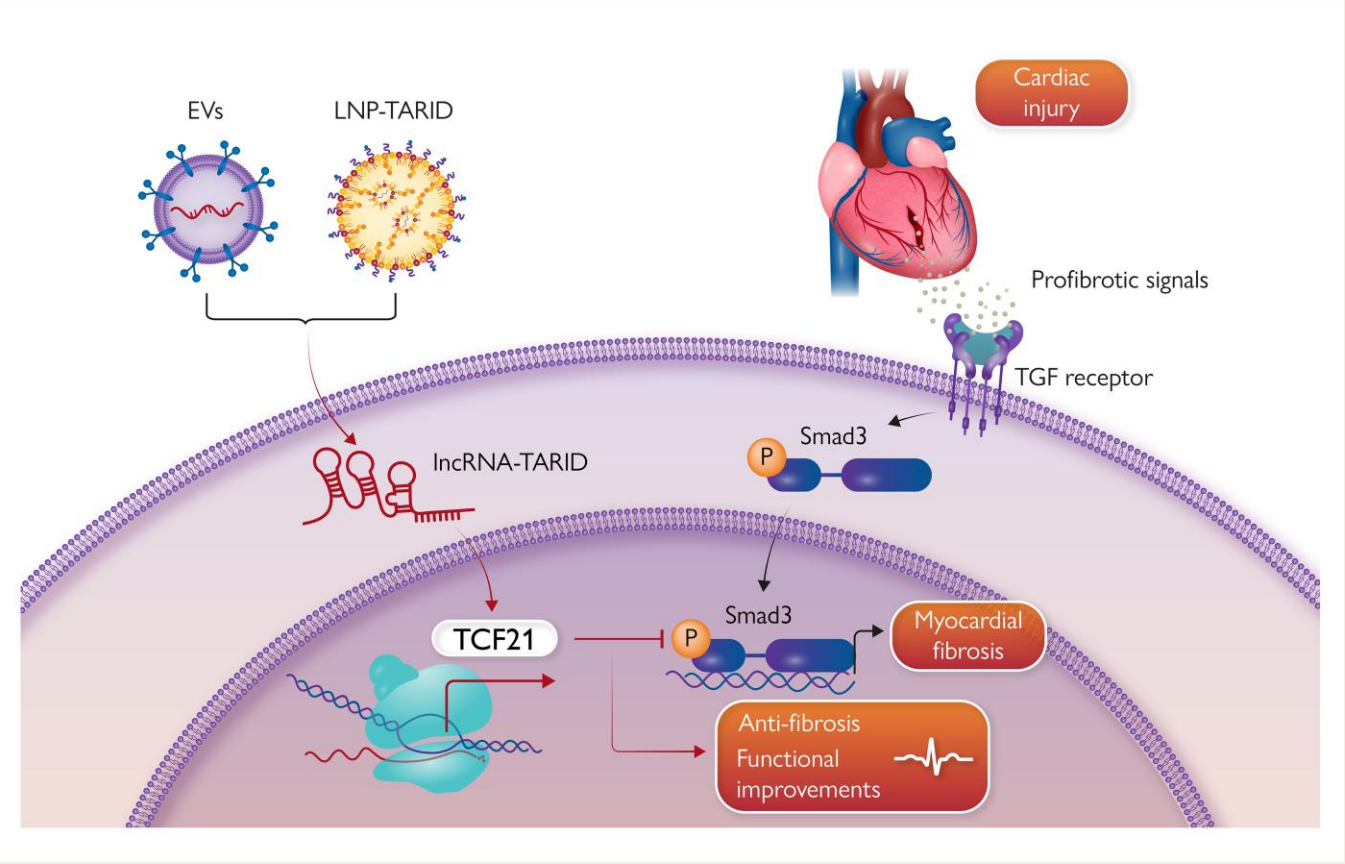

Mesenchymal stem cell–derived extracellular vesicles and LNP–TARID treatment improved myocardial fibrosis by up-regulating *Tcf21* via supplementing lncRNA–TARID. *Tcf21* antagonizes TGF-β/Smad3 signalling pathway to suppress myofibroblast differentiation from epicardial cells. The cardiac histology and function were improved after such therapeutics. EVs, extracellular vesicles; lncRNA, long non-coding RNA; LNP–TARID, lncRNA–TARID laden lipid nanoparticles.

Keywords Myocardial infarction • Adverse remodelling • Mesenchymal stem cell • EVs • lncRNA • *Tcf21*

Translational perspective

Epicardium and epicardium-derived cells (EPDCs) are potential targets for improving cardiac outcomes after myocardial infarction. Intrapericardial injection of therapeutics with hyaluronic acid hydrogel can achieve highly efficient epicardium- and EPDCs-targeted delivery. Through intrapericardial delivery of MSC EVs, this study provides novel insights into the mechanisms underlying MSC-EVs therapy for improving cardiac remodelling and identifies *Tcf21* as a potential target for cardiac repair. Up-regulating *Tcf21* expression by using long non-coding RNA–TARID-laden lipid nanoparticles could be a promising therapeutic approach for the treatment of myocardial fibrosis.

Introduction

Heart disease is the leading cause of death across the world.[1] Coronary artery disease (CAD), the most common type of heart disease, can lead to heart attack and sudden death,[2] while the surviving patients will progress to cardiomyopathy and heart failure (HF) that are associated with myocardial fibrosis.[3,4] Myocardial fibrosis leads to poor outcomes.[5] Currently, there are no specific drugs for treating cardiac fibrosis.[4–8]

Pathologically, the progression of myocardial fibrosis is characterized by the generation of myofibroblasts, which secrete large amount of collagens resulting in stiffness of the myocardium.[9,10] The majority of myofibroblasts arise from cardiac intrinsic fibroblasts,[11] whose developmental origin traces back to the epicardium.[12–15] In the adult heart, epicardium can be reactivated in response to injury, and epicardium-derived cells (EPDCs) differentiate into myofibroblasts that structurally support the necrotic myocardium which lately turns into a fibrotic scar.[13,16] These pathological roles make epicardium and EPDCs potential targets for anti-fibrotic therapies.

The benefits of cell therapy to anti-fibrosis have been well documented,[17,18] and the underlying mechanisms have been attributed to paracrine effects of mesenchymal stem cells (MSC).[19] Extracellular vesicles (EVs) carrying microRNAs, long non-coding RNAs (lncRNA), and growth factors are the major players in paracrine effects.[20] However, clinical application of EVs is hindered by challenges in large-scale production, standardization,[21] and quality control as well as lack of understanding of the complicated cargos of EVs.[22] Identification of functional cargos underlying the therapeutic effects of EVs can lead to rational new drug design and revolutionize cardiovascular regenerative medicine.

In our previous studies, intrapericardial (iPC) injection of MSC-derived EVs improved cardiac remodelling after myocardial infarction (MI).[23–25] Intrapericardial-injected EVs were uptake by EPDCs.[24] We therefore investigated the effects of iPC-injected MSC EVs on EPDC differentiation and explored the underlying mechanisms. Through RNA-seq and gene-set enrichment analysis, we identified *Tcf21* as a potential target to suppress the profibrotic differentiation of EPDCs. In searching for the upstream regulators of *Tcf21*, we found that one particularly EV cargo, lncRNA–*Tcf21* antisense RNA inducing demethylation (TARID), was able to up-regulate *Tcf21* expression. Synthetized lipid nanoparticle (LNP) laden with lncRNA–TARID (LNP–TARID) could up-regulate *Tcf21* expression in EPDCs and inhibit their profibrotic differentiation. Additionally, iPC injection of LNP–TARID suppressed myocardial fibrosis and improved cardiac electrophysiological properties in both mouse and pig models of cardiac injury. Taken together, this study revealed novel mechanisms underlying the anti-fibrotic effects of MSC EVs and developed a potential lncRNA therapy that targets *Tcf21* for myocardial fibrosis treatment.

Methods

Preparation of hyaluronic acid hydrogel

Medical grade (endotoxins < 0.02 IU/mg) hyaluronic acid (HA) hydrogel was used to prolong the retention of EVs.[24] Sodium hyaluronate powder (2000 KDa) was purchased from Echelon Biosciences (H-2000, USA). To prepare the injectable HA hydrogel, sodium hyaluronate powder was dissolved in deionized water to allow complete hydration. After balancing at 4°C overnight, the HA hydrogel (10 mg/mL) can be used for injection. The scanning electron microscope (SEM) images of HA hydrogel were acquired after lyophilization by using a benchtop SEM (JCM-7000, Jeol).

Mesenchymal stem cell culture and extracellular vesicle isolation

Human umbilical cord–derived MSCs (hMSC) were purchased from the American Type Culture Collection (ATCC, Catalog#: PCS-500-010) and cultured with 10% fetal bovine serum (FBS)–containing Iscove's modified Dulbecco's medium (IMDM). After three passages, serum-free medium was changed for conditioned medium collection. To isolate EVs, conditioned medium was filtered through a 0.22 μm filter to exclude cellular debris, followed by passing through the KrosFlo® KR2i Tangential Flow Filtration (TFF) System (Repligen, USA) that equipped with a 300 KDa filter. Characterization of EVs (1:1000 dilution, buffered with PBS) was performed by Nanosight (NS300, Malvern Panalytical) with the indicated settings (see Supplementary data online, *Table S1*), and western blot detection of CD9 and CD81. Laemmli Sample Buffer (Bio-Rad, catalog #1610747) was used for protein extraction, and a 4%–20% gradient polyacrylamide gel (Bio-Rad, catalog#4568093) was used for SDS-PAGE, with Tris/glycine/SDS running buffer (Bio-Rad, catalog#1610732). To acquire transmission electron microscopy (TEM) images, EVs were fixed with 4% paraformaldehyde (PFA) for 5 min at room temperature, followed by loading onto a 200-mesh copper grid and negative staining with 1% uranyl acetate (UA) solution. After two washes with distilled water and air drying, the samples were used for TEM imaging (JEOL 2000FX TEM).

Biodistribution of extracellular vesicles after intrapericardial injection

D-Luciferase catalyzed bioluminescence is a reliable method for *in vivo* tracking of EVs.[26] Immediately after left anterior descending artery (LAD) ligation, 10^{10} EVs in 20 μL PBS or HA hydrogel were injected into the pericardial cavity. Under general anaesthesia with isoflurane inhalation (2% in oxygen), D-luciferin (XenoLight™ D-Luciferin K^+ salt) was intraperitoneally injected (150 mg/kg body weight), and images were acquired 5 min after D-luciferin injection. In addition, EVs labelled with DiD (10 μM) were used for *in vivo* assessment of cellular uptake.[27]

lncRNA synthesis and lipid nanoparticle preparation

lncRNA–TARID was synthesized as previously described.[28] Briefly, total RNA acquired from hMSC was used for cDNA synthesis using a commercial kit (Bio-Rad, 1708890). The cDNA was then used for amplification of DNA templates of lncRNA–TARID using a routine *Taq* PCR kit (E5000S, New England Biolabs). Electrophoresis using 0.8% Agarose gel was performed to separate target DNA bands for gel extraction (T1020, New England Biolabs). Purified DNA template was then used for lncRNA–TARID synthesis. *In vitro* transcription of lncRNA–TARID was performed by using the HiScribe™ T7 Quick High Yield RNA Synthesis Kit (E2050S, New England Biolabs), and the concentration of RNA product was measured using the NanoDrop spectrophotometer (ThermoFisher Scientific).

Lipid nanoparticle was prepared according to a previous study.[29] Briefly, ionizable lipids (18:0, 1,2-distearoyl-3-dimethylammonium-propane, DAP, Avanti Catalog#890820), phospholipids (18:0, 1,2-distearoyl-sn-glycero-3-phosphocholine, DSPC, Avanti Catalog#850365), cholesterol (plant derived, Avanti Catalog#700100), and pegylated lipids 1,2-distearoyl-sn-glycero-3-phosphoethanolamine-N-(amino(polyethylene glycol)-2000 (DSPE-PEG2000 Amine, Avanti Catalog#880128) were dissolved in ethanol and mixed at molar ratios of 50:10:38.5:1.5, followed by mixing with the lncRNA solution at a ratio of 1:2.5. LNPs were prepared by passing the mixture through an extruder kit (Avanti). Particle size was characterized using a NanoSight NS300 (Malvern Panalytical).

RNA-seq and quantitative reverse transcription–polymerase chain reaction analysis

Total RNA was extracted using TRIZOL reagent (ThermoFisher, Catalog#5596018, USA). After precipitation, RNA samples were sent to LC Science for bulk RNA-sequencing. RNA-seq analysis was done with RStudio (Version 1.4.1717). Lowly expressed gene filtration and normalization were performed using the edgeR package. Lowly expressed genes were filtered as unexpressed if the average count per million (CPM) is <0.5. Differential expressions were analysed using the Limma package, and the counts were transformed to log2CPM values using voom function. Afterwards, an interactive plot of the differentially expressed genes was acquired via the glMDPlot function in the Glimma package, and the subset gene-of-interest across the groups were selected for analysis.

To perform quantitative reverse transcription–polymerase chain reaction (qRT–PCR) analysis, cDNA was first synthesized using iScript™ cDNA synthesis kit (1708890, Bio-Rad). Then the cDNA samples were used for qRT–PCR detection of target gene expression using SsoAdvanced Universal SYBR Green Supermix (1725271, Bio-Rad). Statistical analysis was calculated by the $2^{-\Delta\Delta Ct}$ equation. The primer pairs used in this study were listed in Supplementary data online, *Table S2*.

Flow cytometry analysis

Flow cytometry was performed by using a LSRII flow cytometer (BD Biosciences). The cells were fixed with 4% PFA for 15 min at room temperature (RT), followed by PBS wash, permeabilization using 0.01% Triton X-100, and primary antibody incubation. The antibody information can be seen from Supplementary data online, *Table S3*. After incubation at RT for 45 min, the cells were washed with PBS and incubated with fluorescent-labelled secondary antibodies for 30 min at RT. After two washes with PBS, the cells can be used for flow cytometry analysis.

Western blot

Samples were lysed in RIPA lysis buffer supplemented with 0.1 mM proteinase inhibitor (PMSF, 36978, Thermo Fisher Scientific). Protein was extracted and quantified by a BCA assay (Catalog number 23225, Thermo Fisher Scientific), followed by denature and electrophoresis using Mini-PROTEAN TGX Stain-Free Precast Gels (Bio-Rad). After that, the samples were transferred to a polyvinylidene difluoride membrane, which was incubated with 5% milk (1706404XTU, Blotting Grade Blocker Nonfat Dry Milk, Bio-Rad) in tris buffered saline with 0.1% tween (w/v) at RT for 1 h, followed by incubation with primary antibodies overnight at 4°C on a shaking platform. After three washes with 0.1% tween 20-containing phosphate-buffered saline, the membranes were incubated with the horseradish peroxidase (HRP)–conjugated secondary antibody for 1 h at RT. Then the enhanced chemiluminescence (ECL) kit (1705061, Bio-Rad) was used for colorization, and images were acquired using the ChemiDoc Imaging System (Bio-Rad).

Lentivirus and siRNA transfection

Recombinant *Tcf21* expressing lentivirus were ordered from Vector Builder. To construct the *Tcf21* overexpressing cell line, EPDCs were transfected with lentivirus at a multiplicity of infection (MOI) of 10 for 12 h. After that, the fresh medium was changed for cell culture for another 48 h. Stable expressing cells were selected using 1 μg/mL puromycin. To knock down the expression of *Tcf21*, siRNA was purchased from Eurofins. The sequence of the siRNA is available in Supplementary data online, *Table S2*.

Subcutaneous implantation model

After collection of the EPDCs, 10^5 cells in 20 μL HA hydrogel were subcutaneously injected in the dorsal skin. Ten days later, the implants were collected for fixation using 10% neutral buffered formalin. After dehydration using 30% glucose, the implants were embedded in Tissue-Tek® O.C.T. Compound for cryosection. A series of sections (5 μm in thickness) were acquired for staining.

Collagen pad contraction assay

A collagen pad contraction assay kit (CBA-201, Cell Biolabs) was used to assess cell contraction. A collagen gel working solution was prepared and placed in an ice bath until use. Cells were collected and resuspended in the working solution to make a cell–collagen mixture, which was added to a 24-well plate (0.5 million cells per well). The plate was incubated at 37°C for 1 h. After collagen polymerization, 1 mL culture medium was added onto the collagen gel lattice for a 2-day incubation with the cells, during which the contraction stress develops. The collagen pad size was measured for quantitative analysis.

Reactive oxygen species and TGF-β stimulation

Reactive oxygen species stress was introduced by incubating cells with 200 μM H_2O_2 for 2 h. The fresh medium was changed for cell culture. To introduce TGF-β stimulation in cells, 10 ng/mL TGF-β was dissolved in basic medium and stored at −80°C until use.

Animal models

Mouse MI model and pig myocardial ischaemia/reperfusion (I/R) injury model were used in this study.[30] The details for animal surgery, groups, sample size, and follow-up span can be found in the Supplementary Method section.

Cardiac function measurement

Cardiac function was measured at indicated time points. After anaesthesia with inhalation of isoflurane, the animals were fixed to the operating plate with body temperature maintained at 37°C. B-mode and M-mode images were collected using an ultrasound machine equipped with a 40 MHz transducer (Prospect T1, S-Sharp, Taiwan). Left ventricular dimensions at both diastole and systole (LVIDd, LVIDs) were measured, and accordingly, left ventricular ejection fraction (LV-EF), left ventricular fraction shortening (LV-FS), and left ventricular volume at end diastole and systole (LV-EDV, LV-ESV) were calculated. Five continuous cardiac cycles were collected from each mouse. For pig measurements, a Philips CX30 ultrasound machine was used. Quantitative data were acquired from three continuous cardiac cycles.

Immunocytochemistry

To perform immunocytochemistry staining, cells were fixed with 4% PFA for 15 min at RT, followed by permeabilization using 0.01% Triton X-100. After two washes with PBS, the cells were incubated with blocking serum at RT for 1 h. Then the primary antibody diluted in normal goat serum containing 0.01% Triton X-100 was added for incubation overnight at 4°C. After washing with PBS, fluorescently conjugated secondary antibodies were added for staining. DAPI-containing mounting media was used to stain the nuclei (P36935, ThermoFisher Scientific).

Data acquisition and statistical analysis

Animals were randomized to treatment groups. Data acquisition and analysis were performed by investigators who were blinded to the groups. The data acquisition and processing software are MS Excel 2016, Image J version 1.8.0, Living image 4.5 (Perkin Elmer), FV31S-SW viewer version 2.4 (Olympus), Echo Revolve version 5.3 (Echo), and Prospect T-1 (S-Sharp, Version 3.132.2094). Statistical analysis was performed using GraphPad Prism 9 (Version 9.0.0.121), and data were expressed as mean ± SD. Unless stated otherwise, comparisons between two groups were performed with unpaired, two-tailed Student *t*-test, while for multiple group comparison, one-way ANOVA and two-way ANOVA with Bonferroni correction was performed. $P < 0.05$ was accepted as the criterion of significance.

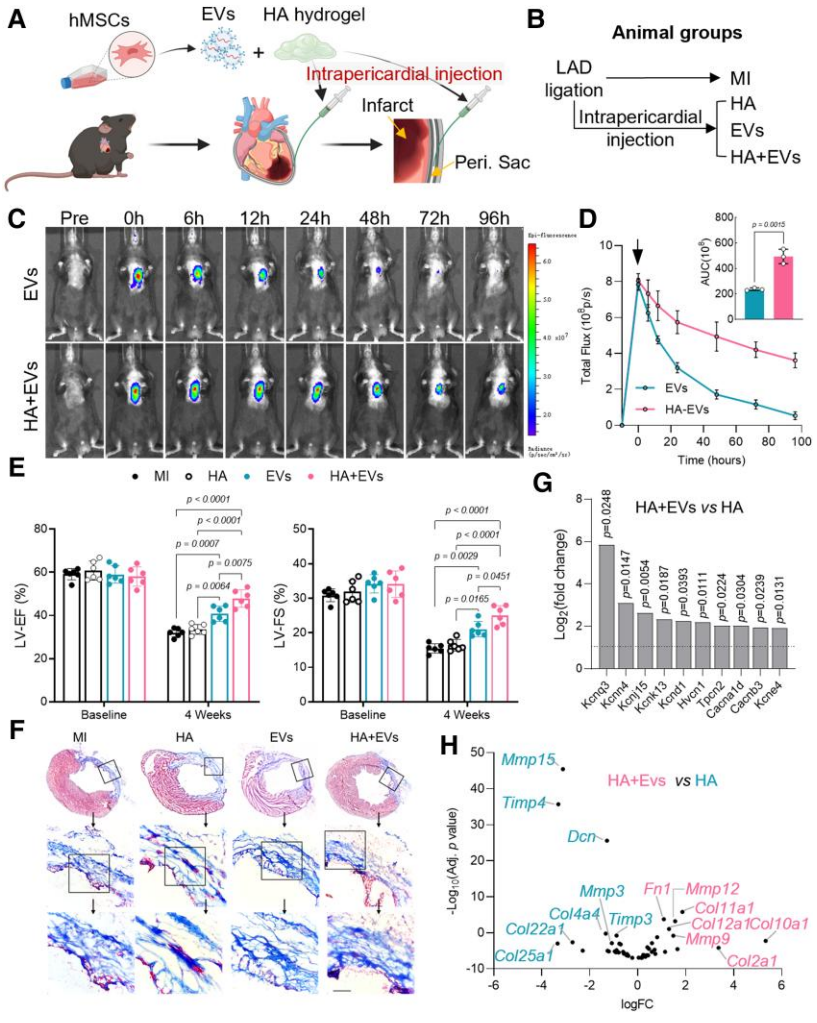

Figure 1 Intrapericardial extracellular vesicle injection improves cardiac function and mitigates cardiac fibrosis. *(A)* Schematic illustration of intrapericardial injection of extracellular vesicles for mice myocardial infarction treatment. Peri. Sac: pericardial sac. *(B)* Treatment groups. *(C)* Live imaging was performed to detect extracellular vesicle biodistribution. *(D)* Quantitative analysis of extracellular vesicles retention in the heart. Data were expressed as mean ± SD, $n = 3$ mice for each group. *(E)* Cardiac function measurement: LV-EF, left ventricular ejection fraction; LV-FS, left ventricular fraction shortening. Data were expressed as mean ± SD, $n = 6$ mice for each group. *(F)* Masson's trichrome staining: blue = scar; pink = viable myocardium. Scale bar, 100 μm. *(G)* The expression of ion channel proteins encoding genes with significant change ($P < 0.05$) was analysed in RNA-seq data. Dash line indicated a fold change of 2. *(H)* RNA-seq analysis of cardiac remodelling–related gene expression with or without EV treatment.

Results

Intrapericardial extracellular vesicle treatment mitigates adverse remodelling after myocardial infarction

Mesenchymal stem cell-derived EVs were iPC injected in mice with MI (*Figure 1A*). Characterization of EVs was performed with TEM, western blot, and NanoSight (see Supplementary data online, *Figure S1A–C*). To enhance EVs retention in the pericardial cavity, medical grade HA hydrogel was prepared for co-injection (*Figure 1A*, Supplementary data online, *Figure S1D*). Immediately after LAD ligation, EVs with or without HA hydrogel were injected into the pericardial space (*Figure 1B*, Supplementary data online, *Figure S1E* and *F*, Supplementary data online, *Video S1*). Co-injection with HA hydrogel prolonged EV retention (*Figure 1C* and *D*). Four weeks after injection, cardiac function and histology were improved as shown by increased values of LV-EF and LV-FS (*Figure 1E*, Supplementary data online, *Figure S2*), and decreased infarct size (*Figure 1F*, Supplementary data online, *Figure S3A–C*). Moreover, the infarct scar of HA + EVs–treated hearts exhibited well-aligned extracellular fibres (*Figure 1F*, Supplementary data online, *Figure S3D* and *E*), which were reportedly associated with improved compliance and reduced arrhythmogenicity.[31,32] Similar results were also found in pig post-MI hearts treated with EVs (see Supplementary data online, *Figure S4*).[33–36] In addition, EVs treatment reduced cardiomyocyte apoptosis and promoted angiogenesis (see Supplementary data online, *Figure S5*). Taken together, the above results showed that EVs treatment mitigated adverse remodelling and improved cardiac repair after MI.

RNA-seq was performed to gain insights into the molecular changes of the infarct scar after HA + EVs treatment. Consistent with the improved cardiac function, we found that cardiac expression of potassium

channel–encoding genes (*Kcnn4, Kcnj15, Kcnk13*, and *Kcne4*),[37–40] hydrogen voltage-gated channel 1 gene (*Hvcn1*),[41] and calcium channel–encoding genes (*Cacna1d* and *Cacnb3*) were up-regulated (*Figure 1G*, Supplementary data online, *Figure S6A*). Those genes have been reported to participate in action potential propagation and electric conduction of ventricular myocytes.[42] Analysis of cardiac remodelling–related gene expression showed increased levels of matrix metalloproteinase (*Mmp9, Mmp12*) in HA+EVs–treated hearts (*Figure 1H*, Supplementary data online, *Figure S6B–F*), while HA-treated hearts showed clear suppression of MMP activities as indicated by elevated expression of tissue inhibitors of MMP (*Timp3, Timp4*) (*Figure 1H*, Supplementary data online, *Figure S6B–F*). Given that increased TIMPs suppress the turnover of extracellular matrix (ECM) components and worsen adverse remodelling,[43,44] our results suggested that EVs treatment promoted ECM component turnover and collagen alignment by increasing MMP activities.

Extracellular vesicle uptake by epicardium-derived cells leads to anti-fibrotic differentiation

The epicardium as the serous layer of the pericardium delineates myocardium.[14,45] After iPC injection, the HA hydrogel formed a patch-like layer covering the epicardium (see Supplementary data online, *Figure S7A*). The EVs were uptake by EPDCs (see Supplementary data online, *Figure S7B* and *C*). Meanwhile, the epicardial layer expanded coinciding with enhanced cell proliferation (see Supplementary data online, *Figure S7D–F*). Epicardium-derived cells play critical roles in cardiac repair via supplementing cells and secreting bioactive factors.[13,45] However, in response to injury, EPDCs undergo epithelial-to-mesenchymal transition (EMT) to become myofibroblasts that cause cardiac fibrosis.[11,13,14] To evaluate the influence of iPC-injected EVs on EPDCs differentiation, we isolated EPDCs via enzymatic digestion (*Figure 2A* and *B*), and their phenotypes were characterized (*Figure 2C* and *D*). There was an increase of EMT as indicated by increased β-catenin expression in EPDCs acquired in MI and HA-treated hearts (*Figure 2C* and *D*). Coinciding with the increased EMT, the expression of epithelial markers (Pan-Cadherin and Pan-Cytokeratin) was decreased (*Figure 2E* and *F*), whereas the number of Vimentin$^+$ mesenchymal cells and α-SMA$^+$ myofibroblasts was increased compared to the sham group (*Figure 2G* and *H*). Treatment with EVs decreased the number of β-catenin$^+$ EPDCs (*Figure 2C* and *D*). The epithelial subpopulations of EPDCs were significantly elevated (*Figure 2E* and *F*), while the Vimentin$^+$ mesenchymal cells showed no detectable change (*Figure 2G*). However, it is worth noting that the ratio of α-SMA$^+$ myofibroblasts was strikingly reduced after EVs injection (*Figure 2H*), which was further confirmed by immunocytochemistry staining and qRT–PCR (*Figure 2I* and *J*, Supplementary data online, *Figure S7G* and *H*). These results suggested that iPC injection of EVs suppressed the myofibrogenic differentiation of EPDCs. In addition, qRT–PCR results showed increased expression of *Mmp2, Mmp8, Mmp9*, and *Mmp12*, and decreased *Timp3*, *Timp4* in isolated EPDCs treated with EVs (*Figure 2J*). Consistent with the RNA-seq data (see Supplementary data online, *Figure S6*), these results implied that the MMPs could be an important mediator to improve cardiac remodelling following the anti-fibrotic phenotype transition of EPDCs.

Extracellular vesicle treatment up-regulates *Tcf21* to inhibit profibrotic TGF-β signalling

To understand the molecular effectors underlying the treatment, we performed RNA-seq analysis to investigate the transcription factors implicated in EPDC differentiation. *Tcf21* was identified as a potential target for improving myocardial fibrosis (*Figure 3A* and *B*). Cardiac expression of *Tcf21* was elevated after EVs treatment (*Figure 3B*). The number of α-SMA$^+$ myofibroblasts in the infarct decreased (*Figure 3C*). These results motivate us to investigate the functions of *Tcf21* in EPDCs differentiation and cardiac remodelling.

First, we established *Tcf21* overexpressing (*Tcf21*$^{o/e}$) and *Tcf21* knockdown (*Tcf21*^{si}) cell lines using lentivirus transfection and locked nucleic acid (LNA)-siRNA mediated knockdown (*Figure 3D*). Successful lentivirus transfection was confirmed by detecting enhanced green fluorescent protein expression (*Figure 3D*). qRT–PCR and western blot results confirmed the changes in *Tcf21* expression in the established cell lines (*Figure 3E* and *F*). Overexpression of *Tcf21* promoted EPDCs migration (see Supplementary data online, *Figure S8A* and *B*) and protected EPDCs from oxidative stress (see Supplementary data online, *Figure S8C* and *D*), whereas knockdown of *Tcf21* expression reduced cellular mobility (see Supplementary data online, *Figure S8A* and *B*) and exacerbated apoptosis (see Supplementary data online, *Figure S8C* and *D*).

To mimic the post-injury environments, TGF-β was used to stimulate the cells. Under TGF-β incubation, *Tcf21*^{si} cells yield robust α-SMA and periostin expression (*Figure 3G–J*). The activation of TGF-β/Smad3 pathway was evident (*Figure 3K*, Supplementary data online, *Figure S9A–C*). Overexpression of *Tcf21* suppressed the myofibroblasts differentiation of EPDCs (*Figure 3G–K*). The level of phosphorylated Smad3 (*p*-Smad3) was significantly decreased (see Supplementary data online, *Figure S9A–C*), suggesting decreased myofibroblast activation. It has been reported that, myofibroblast transition leads to cellular contraction because of contractile actin expression.[46] A collagen pad contraction assay was performed. The highest contraction of collagen pads was observed in *Tcf21*^{si} EPDCs (see Supplementary data online, *Figure S9D–F*), and correspondingly, the expression of α-SMA and the mRNA levels of *Acta2* were the highest in *Tcf21*^{si} EPDCs (see Supplementary data online, *Figure S9G* and *H*).[47–49] Overexpression of *Tcf21* decreased α-SMA expression, meanwhile the collagen pad contraction ratio was reduced (see Supplementary data online, *Figure S9D–H*).

Using an *in vivo* implantation model, we studied the differentiation behaviours of EPDCs. Cells (WT, *Tcf21*^{oe}, and *Tcf21*^{si}) were subcutaneously injected in HA hydrogel to establish an implantation model (see Supplementary data online, *Figure S10A*). Ten days after injection, those implants were collected for histological analysis. *Tcf21* overexpression reduced α-SMA$^+$ myofibroblast generation (see Supplementary data online, *Figure S10B*), and the implants exhibited well-aligned collagen fibres (see Supplementary data online, *Figure S10C* and *D*). In contrast, *Tcf21*^{si} implants exhibited extensive α-SMA$^+$ cell clusters with collagen bundle deposition (see Supplementary data online, *Figure S10B–D*).[50] Moreover, we detected increased Collagen 1 expression in *Tcf21*^{si} EPDCs following TGF-β treatment, whereas *Tcf21*$^{o/e}$ enhanced MMP9 expression and decreased Collagen 1 expression (*Figure 3L–N*). Taken together, these results indicated the dominating roles of *Tcf21* in suppressing myofibroblast differentiation of EPDCs by antagonizing TGF-β signalling.

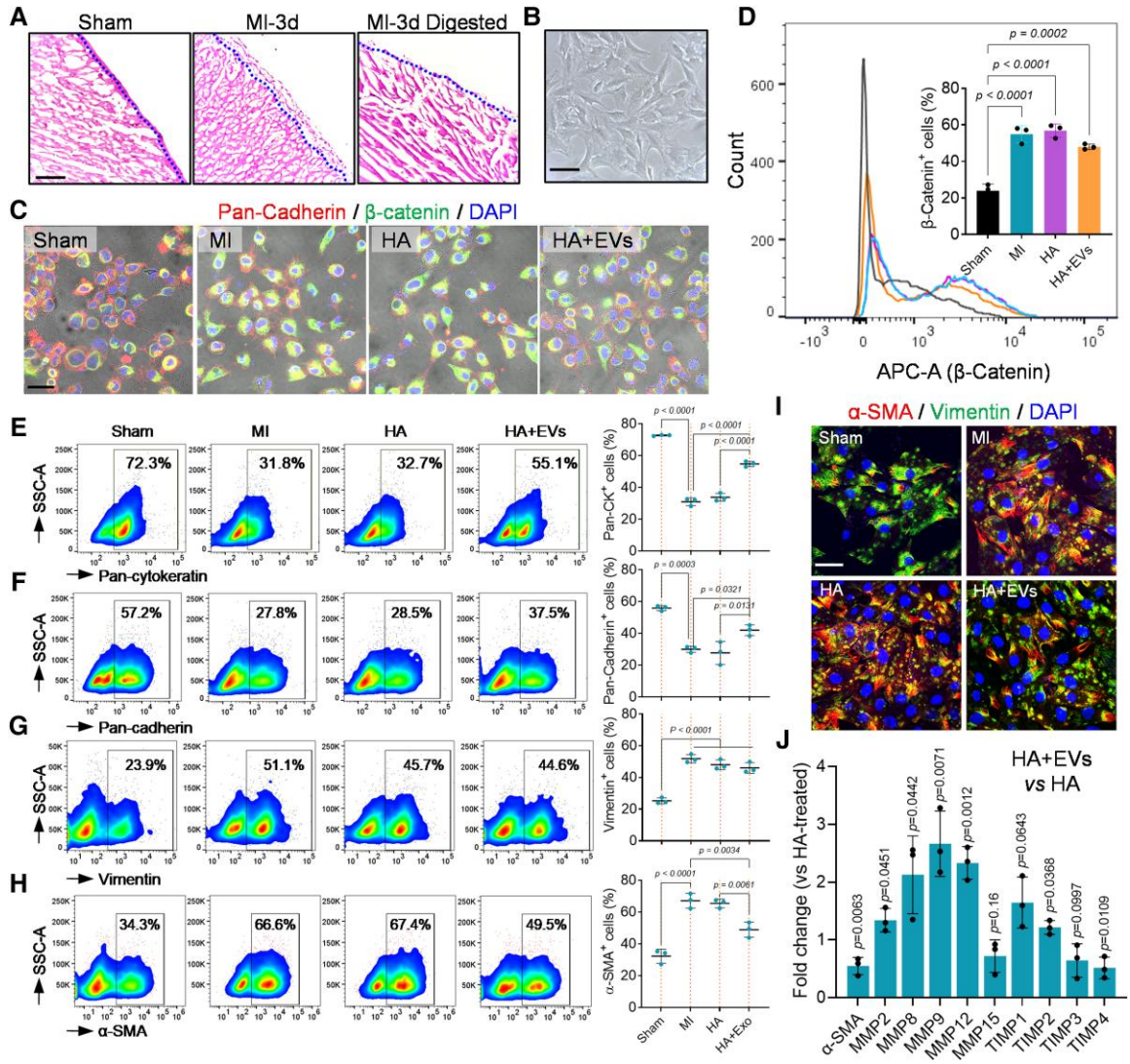

Figure 2 Uptake of extracellular vesicles leads to anti-fibrotic differentiation of epicardium-derived cells. *(A)* Haematoxylin and eosin staining of the heart sections before and after epicardium-derived cell isolation via enzymatic digestion. Scale bar, 60 μm. *(B)* Bright light field image of epicardium-derived cells in culture. Scale bar, 60 μm. *(C)* Immunofluorescence staining of β-Catenin and Pan-Cadherin in isolated epicardium-derived cells. Scale bar, 100 μm. *(D)* Flow cytometry detection of β-Catenin positive cells in indicated groups and the quantitative data. Quantitative data were acquired from triplicated tests and expressed as mean ± SD. *(E–H)* Flow cytometry was performed to characterize the phenotypes of epicardium-derived cells. Quantitative data were acquired from triplicated tests and expressed as mean ± SD. *(I)* Immunofluorescence staining of α-SMA and Vimentin in isolated epicardium-derived cells. Scale bar, 40 μm. *(J)* Quantitative reverse transcription–polymerase chain reaction detection of MMPs and TIMPs expression in epicardium-derived cells. Data were acquired from triplicated tests and expressed as mean ± SD.

Extracellular vesicle cargo lncRNA–TARID up-regulates *Tcf21* expression in epicardium-derived cells

Cellular expression of *Tcf21* is regulated by epigenic modifications, and lncRNA–TARID can activate *Tcf21* expression.[51,52] We therefore detected the expression of lncRNA–TARID in MSCs and EVs (*Figure 4A*) and investigated its potential roles in inducing *Tcf21* expression in EPDCs. The expression of lncRNA–TARID in MSCs was increased after serum depletion (*Figure 4A*), suggesting a stress-induced up-regulation.[53,54] Knockdown of lncRNA–TARID in MSCs using siRNA decreased lncRNA–TARID levels in EVs (*Figure 4A*, Supplementary data online, *Figure S11A and B*); meanwhile, the cellular expression of *Tcf21* was decreased (*Figure 4B and C*), suggesting a positive correlation between lncRNA–TARID and *Tcf21* expression.

Extracellular vesicles depleted with lncRNA–TARID were further used for EPDCs treatment, under the conditions of reactive oxygen species (ROS) stress and TGF-β stimulation.[23] Incubation with TGF-β decreased *Tcf21* expression in EPDCs (*Figure 4D and E*), and the expressions of *Smad3*, *Acta2*, and *Myocd* were robustly increased (*Figure 4F–H*). Treatment with EVs up-regulated *Tcf21* expression (*Figure 4E*) and inhibited myofibroblast differentiation (*Figure 4F–H*). Conversely, depletion of lncRNA–TARID abolished the anti-fibrotic benefits of EVs (*Figure 4E–H*).

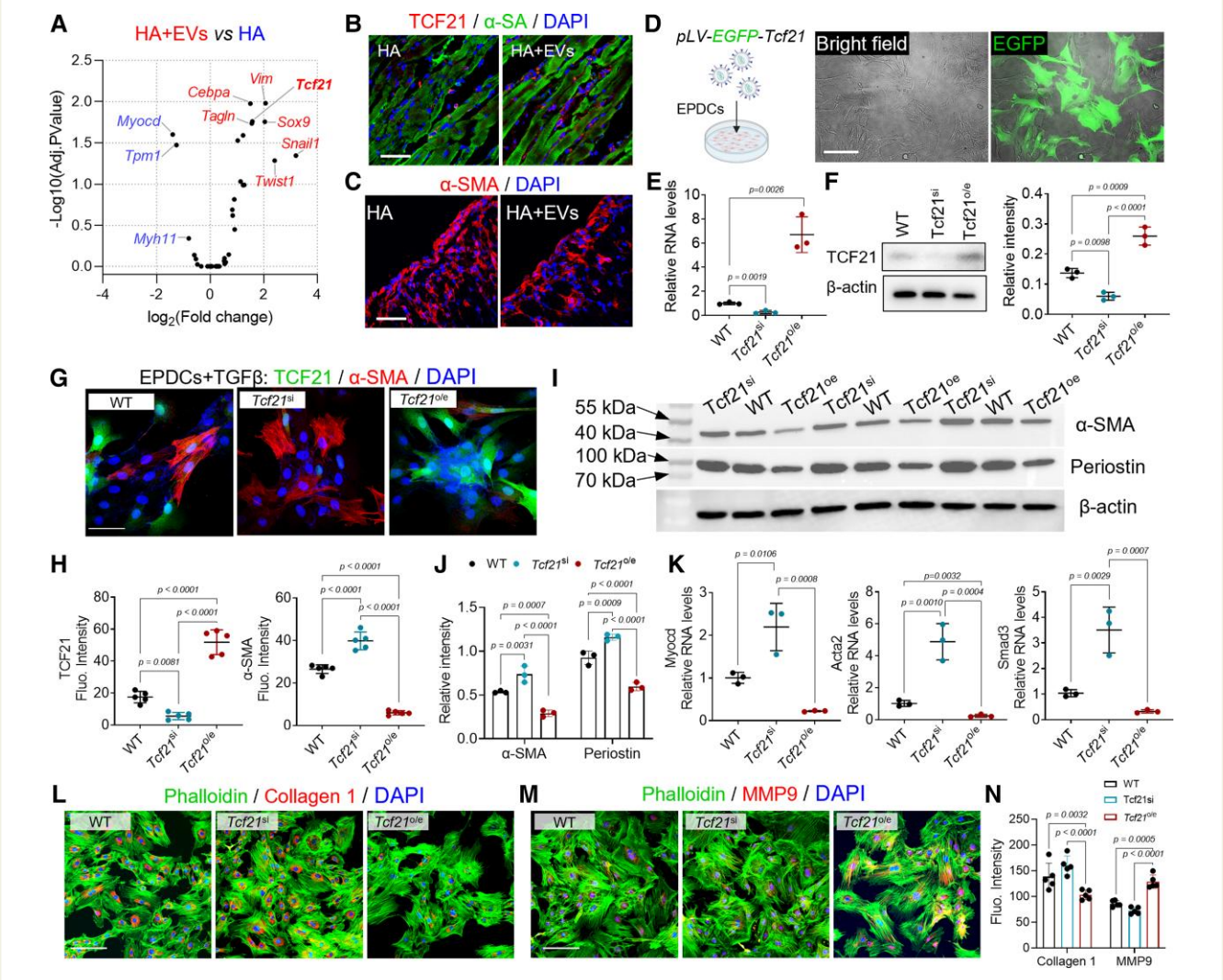

Figure 3 Extracellular vesicle treatment up-regulates *Tcf21* to inhibit profibrotic TGF-β signalling. (*A*) RNA-seq analysis of epicardial cell differentiation–related gene expression. (*B–C*) Immunofluorescence staining of *Tcf21* and α-SMA in the infarct. Scale bar, 60 μm. (*D*) Establishment of *Tcf21* overexpressing (*Tcf21*^{oe}) epicardium-derived cells' cell line through lentivirus transfection. The transfection was confirmed by detecting green fluorescent protein expression. Scale bar, 60 μm. (*E*) Relative gene expression of *Tcf21* in established cell lines. Data were acquired from triplicated tests and expressed as mean ± SD. (*F*) Western blot detection of *Tcf21* expression in established epicardium-derived cells' cell lines. (*G*) Immunofluorescence staining of *Tcf21* and α-SMA in epicardium-derived cells after TGF-β incubation, and accordingly the fluorescent intensity (Fluo. Intensity) was measured for quantitative analysis (*H*). Data are expressed as mean ± SD. Quantitative data were acquired from five images in each group. Scale bar, 60 μm. (*I*) Western-blot detection of α-SMA and periostin expression and (*J*) the quantitative data. (*K*) Quantitative reverse transcription–polymerase chain reaction detection of *Myocd, Acta2*, and *Smad3* expression in epicardium-derived cells. Data were acquired from triplicated tests and expressed as mean ± SD. (*L–N*) Immunostaining detection of Collagen 1 and MMP9 expression in epicardium-derived cells and the quantitative data (*N*). Quantitative data were acquired from five images in each group and expressed as mean ± SD. Scale bar, 60 μm.

To confirm that the observed effects are caused by lncRNA–TARID, we performed gain-of-function study (see Supplementary data online, *Figure S11C*). LncRNA–TARID-laden LNPs (LNP–TARID) were used for *in vitro* studies[28] (*Figure 4I* and *J*, Supplementary data online, *Figure S11D*, Supplementary data online, *Figure S12*). Supplement of LNP–TARID significantly elevated *Tcf21* expression in EPDCs (*Figure 4K* and *L*, Supplementary data online, *Figure S11C*). LNP–TARID treatment suppressed the expression of *Myocd and Acta2* (α-SMA) in TGF-β incubated EPDCs (*Figure 4M* and *N*). Taken together, these results revealed the anti-fibrotic functions of lncRNA–TARID in mediating the anti-fibrotic effects of EVs via up-regulating *Tcf21* expression.

Therapeutic potential of LNP–TARID in mice with myocardial infarction

We went ahead to explore the therapeutic effects of LNP–TARID in a mouse model of acute MI. After modelling, LNP–TARID was injected to the pericardial cavity with HA hydrogel (*Figure 5A*). Uptake of LNP–TARID increased *Tcf21* expression in the epicardial cells (*Figure 5B*, Supplementary data online, *Figure S13A*). Characterization of isolated EPDCs by flow cytometry indicated inhibited myofibroblast differentiation (see Supplementary data online, *Figure S13B* and *C*). Moreover, western blot results showed

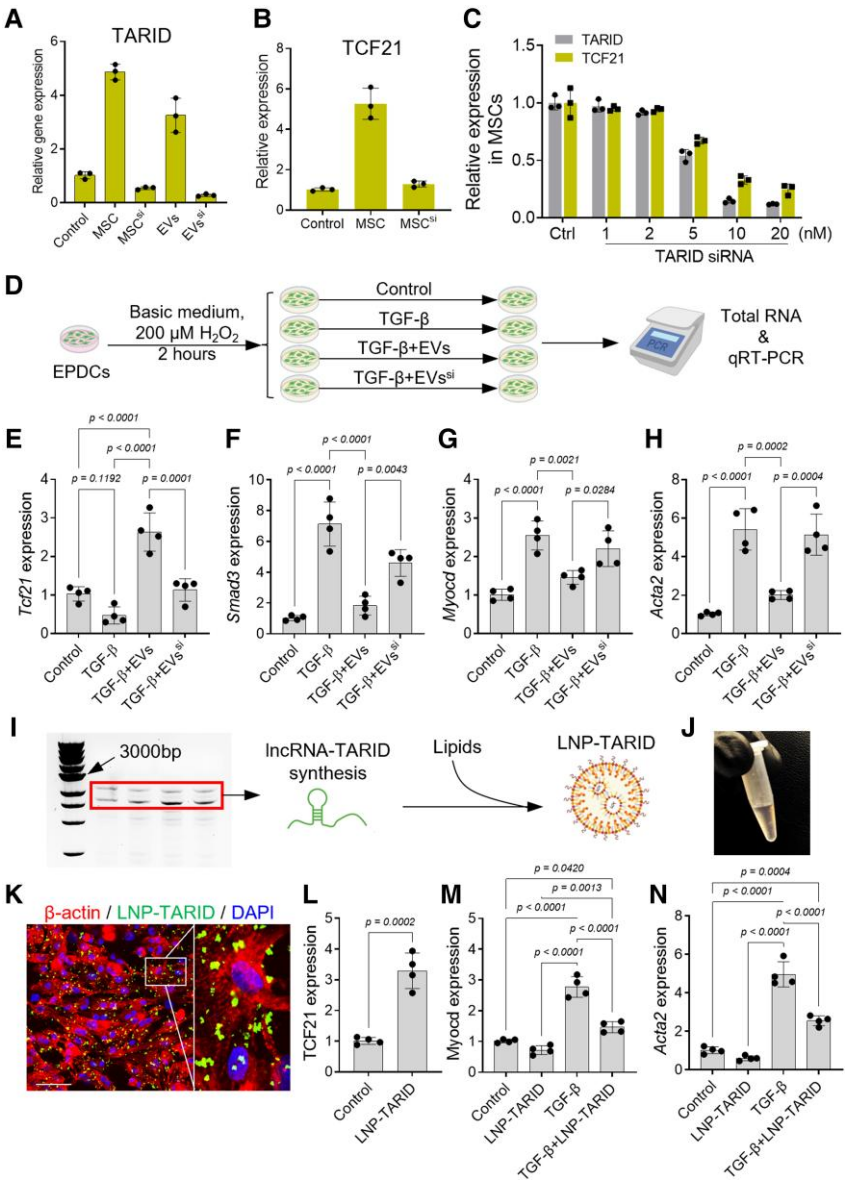

Figure 4 lncRNA–TARID up-regulates *Tcf21* expression in epicardium-derived cells. (*A*) Quantitative reverse transcription–polymerase chain reaction detection of lncRNA–TARID expression in mesenchymal stem cell and mesenchymal stem cell-derived extracellular vesicles. (*B*) Quantitative reverse transcription–polymerase chain reaction detection of *Tcf21* expression in mesenchymal stem cells. (*C*) Relative levels of lncRNA–TARID and *Tcf21* expression after locked nucleic acid–mediated lncRNA–TARID knockdown in mesenchymal stem cells. Scrambled locked nucleic acid was used as control (Ctrl). Data are expressed as mean ± SD. Quantitative data were acquired from three independent tests. (*D*) Schematic study design for investigating the functions of lncRNA–TARID in mediating the anti-fibrotic effects of extracellular vesicles. (*E–H*) Quantitative reverse transcription–polymerase chain reaction detection of *Tcf21*, *Smad3*, *Myocd*, and *Acta2* expression in epicardium-derived cells. Quantitative data were acquired from four independent experiments and expressed as mean ± SD. (*I*, *J*) Synthesis of lncRNA–TARID for LNP–TARID preparation. (*K*, *L*) Uptake of LNP–TARID increased *Tcf21* expression in epicardium-derived cells. Scale bar, 60 μm. Quantitative data were acquired from four independent experiments and expressed as mean ± SD. (*M–N*) Quantitative reverse transcription–polymerase chain reaction detection of *Myocd* and *Acta2* expression in epicardium-derived cells after LNP–TARID treatment. Quantitative data were acquired from four independent experiments and expressed as mean ± SD.

decreased Smad3 activation in EPDCs after LNP–TARID therapy (see Supplementary data online, *Figure S13D, E and F*). Four weeks after LNP–TARID treatment, cardiac ejection function was improved (*Figure 5C* and *D*, Supplementary data online, *Videos S2* and *S3*, Supplementary data online, *Figure S14A*). The left ventricle of control LNP-treated mice was enlarged showing features of dilated cardiomyopathy (*Figure 5C* and *D*), whereas LNP–TARID treatment suppressed cardiac dilation (*Figure 5D*), reduced cardiac infarct size

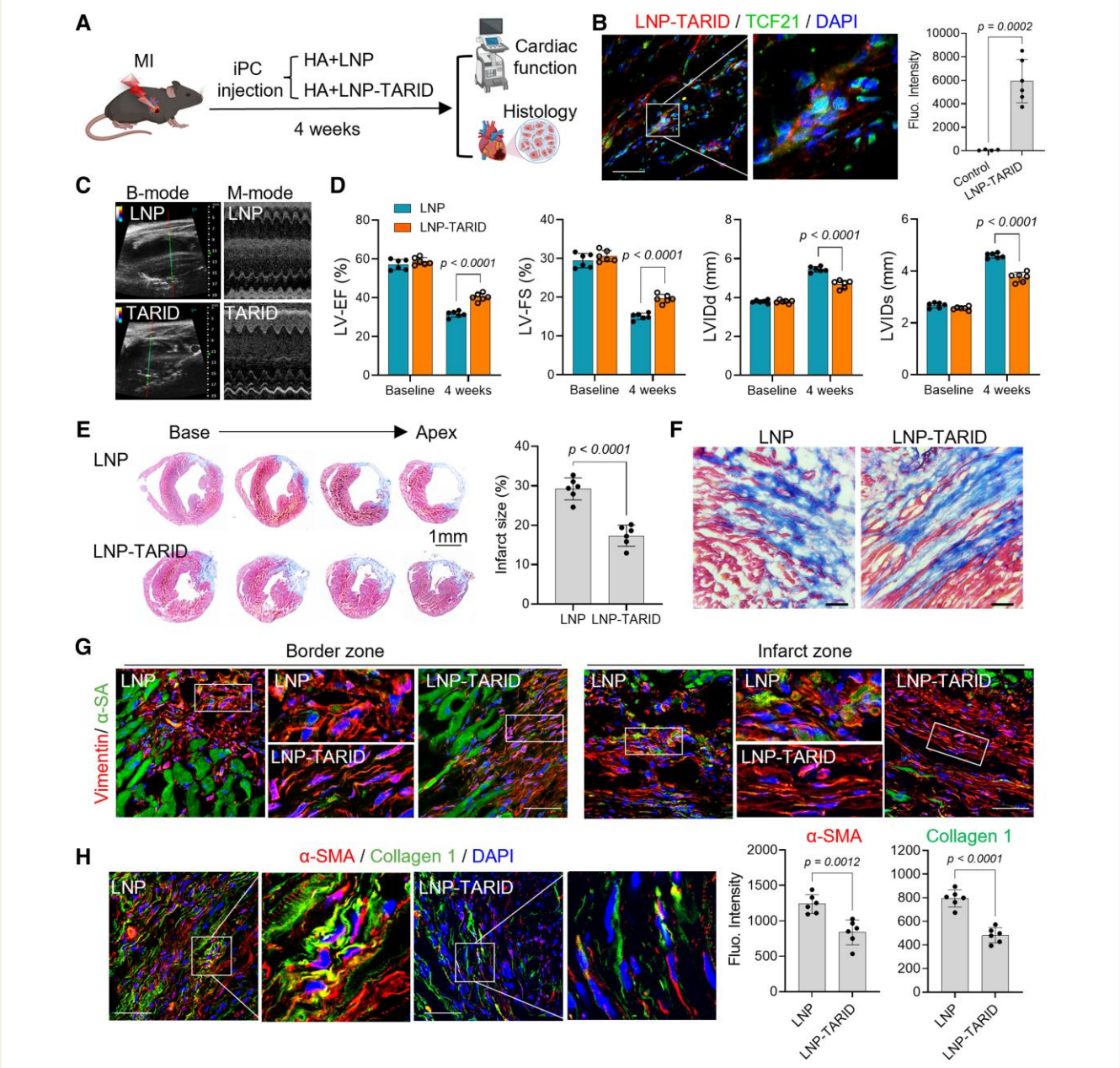

Figure 5 Therapeutic potential of LNP–TARID in mice with myocardial infarction. *(A)* Schematic study design. Immediately after left anterior descending artery ligation, LNP–TARID in hyaluronic acid hydrogel was injected into the pericardial cavity. Empty lipid nanoparticles were used as control. Four weeks after injection, therapeutic efficacy was evaluated by functional and histological analysis. *(B)* Injection of LNP–TARID promoted *Tcf21* expression in myocardial infarction hearts. Scale bar, 60 μm. *(C)* B-mode and M-mode images of echocardiography measurement of cardiac function. *(D)* Quantitative data of cardiac function. Data were expressed as mean ± SD, $n = 6$ mice for each group. *(E)* Masson trichrome staining was performed to show the infarct scar, and accordingly, infarct size was calculated. Quantitative data were expressed as mean ± SD, $n = 6$ mice for each group. *(F)* Comparison of the scar organization in the border zone of the infarct. Scale bar, 60 μm. *(G)* Immunofluorescence staining of Vimentin to show the alignment of fibroblast in the infarct. Scale bar, 60 μm. *(H)* Immunofluorescence staining of α-SMA and Collagen 1 expression in the scar and quantitative analysis. Scale bar, 60 μm. Data were expressed as mean ± SD, $n = 6$ mice for each group.

(*Figure 5E*), and improved collagen and fibroblast alignment (*Figure 5F and G*). Myocardial expressions of α-SMA and Collagen 1, which contribute to scar stiffness,[55] were decreased after LNP–TARID treatment (*Figure 5H*). Additionally, the electrophysiological properties of the hearts were improved (see Supplementary data online, *Figure S14B*).

Therapeutic potential of LNP–TARID in pigs with myocardial infarction

We further investigated the therapeutic efficacy of LNP–TARID in a clinically relevant porcine model of myocardial I/R. Pig I/R model was established via an interventional balloon catheter,[56] which was inflated

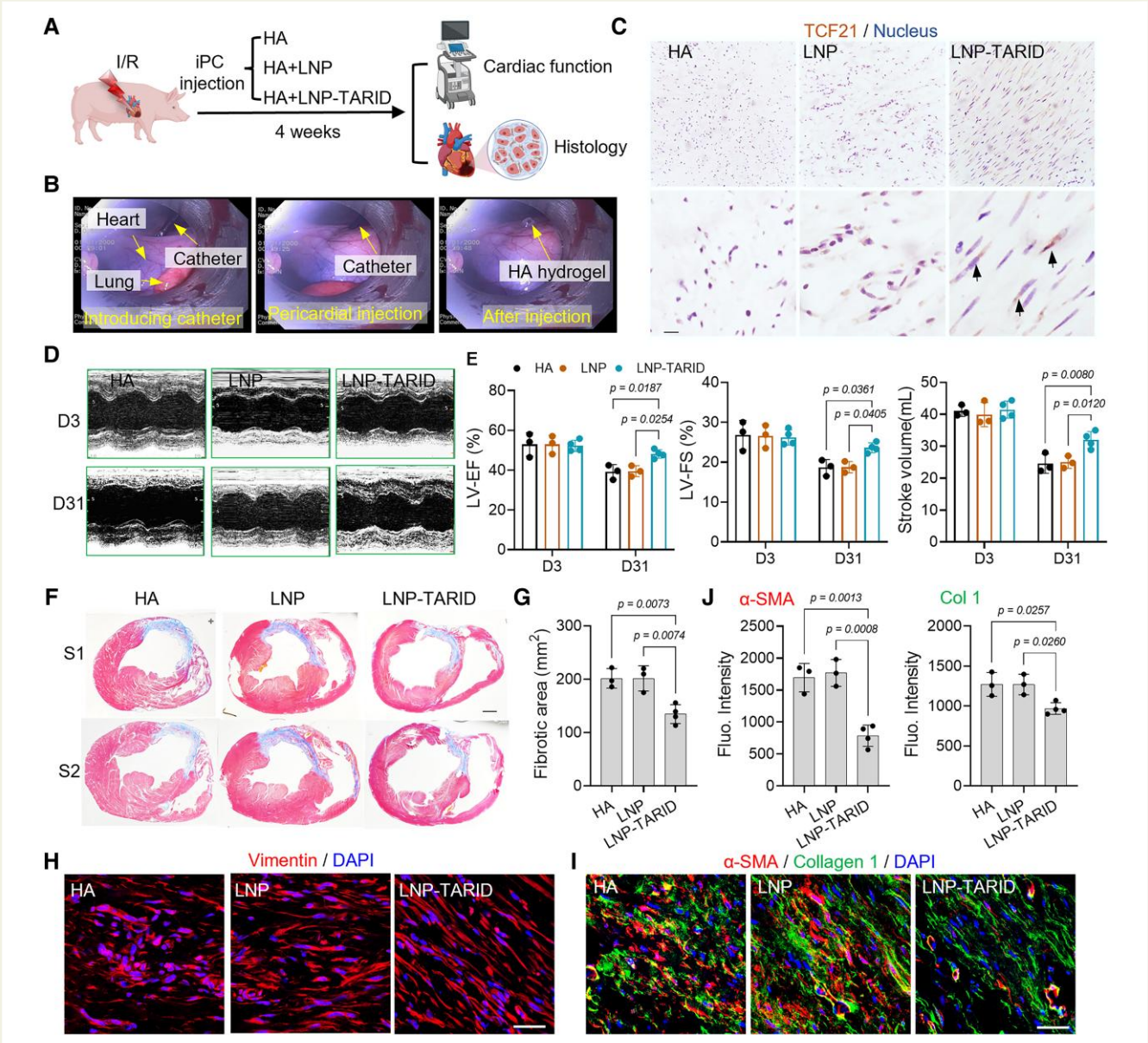

Figure 6 Therapeutic potential of LNP–TARID in pig ischaemia/reperfusion injury. (*A*) Schematic study design. Immediately after reperfusion, LNP–TARID was intrapericardially injected, and hyaluronic acid hydrogel was used as the carrier. Injection of hyaluronic acid hydrogel and empty lipid nanoparticles were used as control. Four weeks after injection, the therapeutic efficacy was evaluated by functional and histological analysis. (*B*) Distilled images showing minimally invasive intrapericardial injection in pigs. (*C*) Immunohistochemistry staining of *Tcf21* in the heart. Scale bar, 100 μm (*D*) M-mode images of echocardiographic measurement of cardiac function. (*E*) Quantitative data to show the left ventricular ejection fraction, left ventricular fraction shortening, and stroke volume changes after LNP–TARID treatment. Data were acquired from three continuous cardiac cycles and expressed as mean ± SD, $n = 3$ pigs in HA and empty LNP treated groups; $n = 4$ pigs in LNP–TARID treated group. (*F*) Masson trichrome staining was performed to show the infarct scar, and accordingly, the fibrotic area (*G*) was measured. Scale bar, 1 cm. Quantitative data were expressed as mean ± SD, $n = 3$ pigs in hyaluronic acid and empty lipid nanoparticle–treated groups; $n = 4$ pigs in LNP–TARID treated group. (*H*) Immunofluorescence staining of Vimentin to show the fibroblasts alignment. Scale bar, 60 μm. (*I*) Immunofluorescence staining to detect α-SMA and Collagen 1 expression in the scar and the quantitative data (*J*). Scale bar, 60 μm. Quantitative data were expressed as mean ± SD, $n = 3$ pigs in hyaluronic acid and empty lipid nanoparticle–treated groups; $n = 4$ pigs in LNP–TARID treated group.

to block the second diagonal branch of the LAD for 90 min (see Supplementary data online, *Figure S15A*). Successful modelling was confirmed by electrocardiography (ECG) and an elevation of plasma troponin levels (see Supplementary data online, *Figure S15B* and *C*). Immediately after reperfusion, pigs received iPC injection of LNP–TARID (*Figure 6A* and *B*, Supplementary data online, *Video S4*). LNP–TARID treatment increased myocardial expression of *Tcf21* (*Figure 6C*), promoted cardiac function recovery (*Figure 6D* and *E*, Supplementary data online, *Figure S15D*), and reduced myocardial infarct size (*Figure 6F* and *G*). In addition, alignment of extracellular

collagens and the cardiac fibroblasts were improved (*Figure 6H*, Supplementary data online, *Figure S16A–C*) that are associated with improved compliance and reduced arrhythmogenicity.[32] Moreover, the expressions of α-SMA and Collagen 1 were decreased after LNP–TARID treatment (*Figure 6I and J*), suggesting improved cardiac remodelling. Myocardial expression of Cx43 was enhanced by LNP–TARID treatment (see Supplementary data online, *Figure S17A and B*), and ECG measurement showed obvious improvement in cardiac electrical conduction (see Supplementary data online, *Figure S17C*). Taken together, our results above suggested improved cardiac functional outcomes in pigs after LNP–TARID treatment.

Discussion

Cardiovascular disease is still the leading cause of death across the world. After cardiac injury, a fibrotic scar takes the place of lost cardiomyocytes. The physical and physiological characters of the scar impact cardiac outcomes.[57] A well-organized scar complies with cardiac contraction and postpones the transition of heart failure. Stiffness of the scar is associated with arrhythmogenicity that leads to sudden cardiac death.[58] Anti-fibrotic therapies are promising to improve outcomes of patients with chronic heart disease.[59,60] In our study, iPC injection of LNP–TARID suppressed the profibrotic differentiation of EPDCs and fibroblasts. The cardiac functional and electrophysiological properties were improved in both mouse and pig models of MI. This approach yielded anti-fibrotic effects, establishing the therapeutic potentials of LNP–TARID for myocardial fibrosis (*Structured Graphical Abstract*).

Tcf21 has long been regarded as a marker of cardiac fibroblasts due to its roles in fibroblast specification during heart development.[15] Persistent expression of *Tcf21* inhibits the differentiation of EPDCs towards smooth muscle cells during development,[15,61,62] meanwhile maintaining EPDCs with stem/progenitor cell features.[63] However, during the differentiation of cardiac fibroblasts into myofibroblast, the expression of *Tcf21* was suppressed by profibrotic signals.[63] The functions of *Tcf21* in cardiac repair remain unknown. The expression of *Tcf21* was regulated by epigenetic modifications.[28,51] LncRNAs are promising therapeutics for disease.[64] However, the poor sequence conservation between species has hindered the translational application of the findings in animal studies. LncRNA–TARID was first identified in human genome,[28] and its functions in non-human species were not explored. We therefore compared the *Tcf21* gene sequences (see Supplementary data online, *Figure S12*) in various species regarding the binding region of lncRNA–TARID to activate *Tcf21* transcription.[51] The promoter zone of *Tcf21* gene in all these species is highly conserved with higher GC contents (> 55%) (see Supplementary data online, *Figure S12A*). This conservation implied that demethylation is a dominant factor for initiating *Tcf21* gene expression.[28] The binding site analysis revealed the homogeneity of the sequences among species.[65,66] *In vitro* transfection of lncRNA–TARID elevated *Tcf21* expression in mouse and pig cells. These results suggested the capability of human lncRNA–TARID to up-regulate *Tcf21* expression in mouse and pig cells.

Earlier studies suggested that epicardium and EPDCs are important players in myocardial fibrosis.[14,45] Epicardium is the developmental origin of cardiac fibroblasts. In the setting injury and stress, EPDCs transdifferentiate into myofibroblasts, resulting in myocardial fibrosis. Interventions to ablate myofibroblasts could lead to a decrease in cardiac fibrosis.[67] In this study, the iPC injection approach achieved epicardial cell-targeted delivery of therapeutics. After iPC injection, the uptake of EVs and LNPs by epicardial cells was evident (see Supplementary data online, *Figure S7B and C*; *Figure 5B* and Supplementary data online, *Figure S13A*). Those therapeutics inhibited the differentiation of EPDCs towards profibrotic myofibroblasts. In this process, the up-regulation of *Tcf21* played a dominating role (*Figure 3*). Mechanistic studies revealed the inhibitory functions of *Tcf21* in myofibroblast activation (*Figure 3*; Supplementary data online, *Figures S8–S10*).[68] After all, iPC injection of EVs and LNP–TARID suppressed the myofibroblast differentiation from EPDCs via up-regulating *Tcf21*.

In this study, the RNA-seq analysis of cardiac remodelling–related gene expression showed increased MMP (*Mmp9, Mmp12*) levels in EVs-treated hearts (*Figure 1H*, Supplementary data online, *Figure S6B–E*), while the control hearts showed elevated tissue inhibitor of metalloproteinase (*Timp3* and *Timp4*) expressions. TIMPs can suppress ECM turnover and worsen cardiac remodelling.[43,44] The results above indicate that MMPs may help to promote ECM components turnover after MI. Additionally, qRT–PCR results confirmed an increase in MMP expression in EPDCs isolated from EVs-treated hearts (*Figure 2J*), and in *Tcf21*-overexpressing EPDCs (*Figure 3M and N*). Moreover, ECM turnover is accompanied by changes of collagen types, but not a uniform decrease of all types of collagens. Anti-fibrotic differentiation of EPDCs decreased the deposition of Collagen 1 (*Figure 3L*). However, the deposition of Collagen 12 was elevated (see Supplementary data online, *Figure S6E*), which has been reported to promote cardiac repair.[69,70] Taken together, these results indicated that the anti-fibrotic polarization of EPDCs benefits cardiac repair.

Our study has several limitations. The EV products may contain soluble proteins, as we used TFF method to extract components with a molecular weight >300 kDa. This size cutoff will intercept not only EVs but also the soluble proteins. In addition, the sample size in the pig study is relatively small. Future animal studies with larger sample sizes will be needed to further evaluate the therapeutic potentials of LNP–TARID. Overall, the present study established novel mechanisms underlying EVs therapy for improving adverse remodelling and identified *Tcf21* as a critical target for reducing myocardial fibrosis. Moreover, an LNP-based lncRNA therapy was developed and tested for the treatment of cardiac fibrosis.

Author contributions

DZ, SL, ZL and KC conceived and designed the study; KH and KC led acquisition of funding; DZ, SL and KH conducted the experiments; DZ, SL, KH, JL, XM and ZL performed data analysis and interpretation; DZ and KC wrote the manuscript. All authors contributed to the revision of the manuscript.

Acknowledgements

The authors thank the Laboratory Animal Resources (LAR), the Central Procedures Lab (CPL), and the Flow Cytometry and Cell Sorting facility at NC State University for their help with this study.

Supplementary data

Supplementary data is available at *European Heart Journal* online.

Data availability

The data involved in this study are available from the corresponding author upon reasonable request.

Conflict of interest

All authors declare no conflict of interest for this contribution.

Funding

This work was supported by grants from the NIH (HL123920, HL137093, HL144002, HL146153, HL147357, and HL149940, to K.C.) and the American Heart Association (18TPA34230092 and 19EIA34660286 to K.C.; 21CDA855570 to K.H).

References

1. Timmis A, Vardas P, Townsend N, Torbica A, Katus H, De Smedt D, *et al.* European Society of Cardiology: cardiovascular disease statistics 2021. *Eur Heart J* 2022;**43**:716–799. https://doi.org/10.1093/eurheartj/ehab892
2. Vahatalo J, Holmstrom L, Pakanen L, Kaikkonen K, Perkiomaki J, Huikuri H, *et al.* Coronary artery disease as the cause of sudden cardiac death among victims < 50 years of age. *Am J Cardiol* 2021;**147**:33–38. https://doi.org/10.1016/j.amjcard.2021.02.012
3. Webber M, Jackson SP, Moon JC, Captur G. Myocardial fibrosis in heart failure: anti-fibrotic therapies and the role of cardiovascular magnetic resonance in drug trials. *Cardiol Ther* 2020;**9**:363–376. https://doi.org/10.1007/s40119-020-00199-y
4. Lewis GA, Dodd S, Clayton D, Bedson E, Eccleson H, Schelbert EB, *et al.* Pirfenidone in heart failure with preserved ejection fraction: a randomized phase 2 trial. *Nat Med* 2021;**27**:1477–1482. https://doi.org/10.1038/s41591-021-01452-0
5. Chen X, Zhu L, Liu J, Lu Y, Pan L, Xiao J. Greasing wheels of cell-free therapies for cardiovascular diseases: Integrated devices of exosomes/exosome-like nanovectors with bioinspired materials. *Extracell Vesicle* 2022;**1**:100010. http://dx.doi.org/10.1016/j.vesic.2022.100010
6. Cleland JGF, Pellicori P, Gonzalez A. A novel treatment for heart failure targets myocardial fibrosis. *Nat Med* 2021;**27**:1343–1344. https://doi.org/10.1038/s41591-021-01457-9
7. Tschope C, Diez J. Myocardial fibrosis as a matter of cell differentiation: opportunities for new antifibrotic strategies. *Eur Heart J* 2019;**40**:979–981. https://doi.org/10.1093/eurheartj/ehy307
8. Ho CY, Day SM, Axelsson A, Russell MW, Zahka K, Lever HM, *et al.* Valsartan in early-stage hypertrophic cardiomyopathy: a randomized phase 2 trial. *Nat Med* 2021; **27**:1818–1824. https://doi.org/10.1038/s41591-021-01505-4
9. Rodriguez P, Sassi Y, Troncone L, Benard L, Ishikawa K, Gordon RE, *et al.* Deletion of delta-like 1 homologue accelerates fibroblast-myofibroblast differentiation and induces myocardial fibrosis. *Eur Heart J* 2019;**40**:967–978. https://doi.org/10.1093/eurheartj/ehy188
10. Small EM, Thatcher JE, Sutherland LB, Kinoshita H, Gerard RD, Richardson JA, *et al.* Myocardin-related transcription factor-a controls myofibroblast activation and fibrosis in response to myocardial infarction. *Circ Res* 2010;**107**:294–304. https://doi.org/10.1161/CIRCRESAHA.110.223172
11. Kanisicak O, Khalil H, Ivey MJ, Karch J, Maliken BD, Correll RN, *et al.* Genetic lineage tracing defines myofibroblast origin and function in the injured heart. *Nat Commun* 2016;**7**:12260. https://doi.org/10.1038/ncomms12260
12. Smith CL, Baek ST, Sung CY, Tallquist MD. Epicardial-derived cell epithelial-to-mesenchymal transition and fate specification require PDGF receptor signaling. *Circ Res* 2011;**108**:e15–e26. https://doi.org/10.1161/CIRCRESAHA.110.235531
13. Zhou B, Honor LB, He H, Ma Q, Oh JH, Butterfield C, *et al.* Adult mouse epicardium modulates myocardial injury by secreting paracrine factors. *J Clin Invest* 2011;**121**:1894–1904. https://doi.org/10.1172/JCI45529
14. Quijada P, Trembley MA, Small EM. The role of the epicardium during heart development and repair. *Circ Res* 2020;**126**:377–394. https://doi.org/10.1161/CIRCRESAHA.119.315857
15. Acharya A, Baek ST, Huang G, Eskiocak B, Goetsch S, Sung CY, *et al.* The bHLH transcription factor Tcf21 is required for lineage-specific EMT of cardiac fibroblast progenitors. *Development* 2012;**139**:2139–2149. https://doi.org/10.1242/dev.079970
16. Fu X, Khalil H, Kanisicak O, Boyer JG, Vagnozzi RJ, Maliken BD, *et al.* Specialized fibroblast differentiated states underlie scar formation in the infarcted mouse heart. *J Clin Invest* 2018;**128**:2127–2143. https://doi.org/10.1172/JCI98215
17. Dinh PC, Paudel D, Brochu H, Popowski KD, Gracieux MC, Cores J, *et al.* Inhalation of lung spheroid cell secretome and exosomes promotes lung repair in pulmonary fibrosis. *Nat Commun* 2020;**11**:1064. https://doi.org/10.1038/s41467-020-14344-7
18. Barile L, Moccetti T, Marban E, Vassalli G. Roles of exosomes in cardioprotection. *Eur Heart J* 2017;**38**:1372–1379. https://doi.org/10.1093/eurheartj/ehw304
19. Popowski KD, López de Juan Abad B, George A, Silkstone D, Belcher E, Chung J, *et al*. Inhalable exosomes outperform liposomes as mRNA and protein drug carriers to the lung. *Extracell Vesicle* 2022;**1**:100002. http://dx.doi.org/10.1016/j.vesic.2022.100002
20. Zhang S, Zhu D, Mei X, Li Z, Li J, Xie M, *et al*. Advances in biomaterials and regenerative medicine for primary ovarian insufficiency therapy. *Bioact Mater* 2021;**6**:1957–1972. http://dx.doi.org/10.1016/j.bioactmat.2020.12.008
21. Vaka R, Remortel SV, Ly V, Davis DR. Extracellular vesicle therapy for non-ischemic heart failure: A systematic review of preclinical studies. *Extracell Vesicle* 2022;**1**:100009. http://dx.doi.org/10.1016/j.vesic.2022.100009
22. Zhu D, Cheng K. Cardiac cell therapy for heart repair: should the cells be left out? *Cells* 2021;**10**:641. https://doi.org/10.3390/cells10030641
23. Li Z, Zhu D, Hui Q, Bi J, Yu B, Huang Z, *et al.* Injection of ROS-responsive hydrogel loaded with basic fibroblast growth factor into the pericardial cavity for heart repair. *Adv Funct Mat* 2021;**31**:2004377. https://doi.org/10.1002/adfm.202004377
24. Zhu D, Li Z, Huang K, Caranasos TG, Rossi JS, Cheng K. Minimally invasive delivery of therapeutic agents by hydrogel injection into the pericardial cavity for cardiac repair. *Nat Commun* 2021;**12**:1412. https://doi.org/10.1038/s41467-021-21682-7
25. Zhu D, Liu S, Huang K, Wang Z, Hu S, Li J, *et al.* Intrapericardial exosome therapy dampens cardiac injury via activating Foxo3. *Circ Res* 2022;**131**:e135–e150. https://doi.org/10.1161/CIRCRESAHA.122.321384
26. Luo W, Dai Y, Chen Z, Yue X, Andrade-Powell KC, Chang J. Spatial and temporal tracking of cardiac exosomes in mouse using a nano-luciferase-CD63 fusion protein. *Commun Biol* 2020;**3**:114. https://doi.org/10.1038/s42003-020-0830-7
27. Betzer O, Barnoy E, Sadan T, Elbaz I, Braverman C, Liu Z, *et al.* Advances in imaging strategies for in vivo tracking of exosomes. *Wiley Interdiscip Rev Nanomed Nanobiotechnol* 2020;**12**:e1594. https://doi.org/10.1002/wnan.1594
28. Arab K, Park YJ, Lindroth AM, Schafer A, Oakes C, Weichenhan D, *et al.* Long noncoding RNA TARID directs demethylation and activation of the tumor suppressor TCF21 via GADD45A. *Mol Cell* 2014;**55**:604–614. https://doi.org/10.1016/j.molcel.2014.06.031
29. Corbett KS, Edwards DK, Leist SR, Abiona OM, Boyoglu-Barnum S, Gillespie RA, *et al.* SARS-CoV-2 mRNA vaccine design enabled by prototype pathogen preparedness. *Nature* 2020;**586**:567–571. https://doi.org/10.1038/s41586-020-2622-0
30. Zhu D, Hou J, Qian M, Jin D, Hao T, Pan Y, *et al*. Nitrate-functionalized patch confers cardioprotection and improves heart repair after myocardial infarction via local nitric oxide delivery. *Nat Commun* 2021;**12**:677. http://dx.doi.org/10.1038/s41467-021-24804-3
31. Caggiano LR, Lee JJ, Holmes JW. Surgical reinforcement alters collagen alignment and turnover in healing myocardial infarcts. *Am J Physiol Heart Circ Physiol* 2018;**315**:H1041–H1050. https://doi.org/10.1152/ajpheart.00088.2018
32. Thavapalachandran S, Grieve SM, Hume RD, Le TYL, Raguram K, Hudson JE, *et al.* Platelet-derived growth factor-AB improves scar mechanics and vascularity after myocardial infarction. *Sci Transl Med* 2020;**12**:eaay2140. https://doi.org/10.1126/scitranslmed.aay2140
33. Sahoo S, Losordo DW. Exosomes and cardiac repair after myocardial infarction. *Circ Res* 2014;**114**:333–344. https://doi.org/10.1161/CIRCRESAHA.114.300639
34. Gallet R, Dawkins J, Valle J, Simsolo E, de Couto G, Middleton R, *et al.* Exosomes secreted by cardiosphere-derived cells reduce scarring, attenuate adverse remodelling, and improve function in acute and chronic porcine myocardial infarction. *Eur Heart J* 2017;**38**:201–211. https://doi.org/10.1093/eurheartj/ehw240
35. Khan M, Nickoloff E, Abramova T, Johnson J, Verma SK, Krishnamurthy P, *et al.* Embryonic stem cell-derived exosomes promote endogenous repair mechanisms and enhance cardiac function following myocardial infarction. *Circ Res* 2015;**117**:52–64. https://doi.org/10.1161/CIRCRESAHA.117.305990
36. Ong SG, Wu JC. Exosomes as potential alternatives to stem cell therapy in mediating cardiac regeneration. *Circ Res* 2015;**117**:7–9. https://doi.org/10.1161/CIRCRESAHA.115.306593
37. Vigneault P, Parent S, Kanda P, Michie C, Davis DR, Nattel S. Electrophysiological engineering of heart-derived cells with calcium-dependent potassium channels improves cell therapy efficacy for cardioprotection. *Nat Commun* 2021;**12**:4963. https://doi.org/10.1038/s41467-021-25180-8
38. Nerbonne JM, Nichols CG, Schwarz TL, Escande D. Genetic manipulation of cardiac K(+) channel function in mice: what have we learned, and where do we go from here? *Circ Res* 2001;**89**:944–956. https://doi.org/10.1161/hh2301.100349
39. Tamargo J, Caballero R, Gomez R, Valenzuela C, Delpon E. Pharmacology of cardiac potassium channels. *Cardiovasc Res* 2004;**62**:9–33. https://doi.org/10.1016/j.cardiores.2003.12.026
40. Crump SM, Hu Z, Kant R, Levy DI, Goldstein SA, Abbott GW. Kcne4 deletion sex- and age-specifically impairs cardiac repolarization in mice. *FASEB J* 2016;**30**:360–369. https://doi.org/10.1096/fj.15-278754
41. Ma J, Gao X, Li Y, DeCoursey TE, Shull GE, Wang HS. The HVCN1 voltage-gated proton channel contributes to pH regulation in canine ventricular myocytes. *J Physiol* 2022;**600**:2089–2103. https://doi.org/10.1113/JP282126

42. Grant AO. Cardiac ion channels. *Circ Arrhythm Electrophysiol* 2009;**2**:185–194. https://doi.org/10.1161/CIRCEP.108.789081
43. Gill SE, Huizar I, Bench EM, Sussman SW, Wang Y, Khokha R, *et al.* Tissue inhibitor of metalloproteinases 3 regulates resolution of inflammation following acute lung injury. *Am J Pathol* 2010;**176**:64–73. https://doi.org/10.2353/ajpath.2010.090158
44. Iyer RP, Patterson NL, Zouein FA, Ma Y, Dive V, de Castro Bras LE, *et al.* Early matrix metalloproteinase-12 inhibition worsens post-myocardial infarction cardiac dysfunction by delaying inflammation resolution. *Int J Cardiol* 2015;**185**:198–208. https://doi.org/10.1016/j.ijcard.2015.03.054
45. Cao J, Poss KD. The epicardium as a hub for heart regeneration. *Nat Rev Cardiol* 2018;**15**:631–647. https://doi.org/10.1038/s41569-018-0046-4
46. Snider P, Hinton RB, Moreno-Rodriguez RA, Wang J, Rogers R, Lindsley A, *et al.* Periostin is required for maturation and extracellular matrix stabilization of noncardiomyocyte lineages of the heart. *Circ Res* 2008;**102**:752–760. https://doi.org/10.1161/CIRCRESAHA.107.159517
47. Khalil H, Kanisicak O, Prasad V, Correll RN, Fu X, Schips T, *et al.* Fibroblast-specific TGF-beta-Smad2/3 signaling underlies cardiac fibrosis. *J Clin Invest* 2017;**127**:3770–3783. https://doi.org/10.1172/JCI94753
48. Biernacka A, Cavalera M, Wang J, Russo I, Shinde A, Kong P, *et al.* Smad3 signaling promotes fibrosis while preserving cardiac and aortic geometry in obese diabetic mice. *Circ Heart Fail* 2015;**8**:788–798. https://doi.org/10.1161/CIRCHEARTFAILURE.114.001963
49. Goldstein JA, Bogdanovich S, Beiriger A, Wren LM, Rossi AE, Gao QQ, *et al.* Excess SMAD signaling contributes to heart and muscle dysfunction in muscular dystrophy. *Hum Mol Genet* 2014;**23**:6722–6731. https://doi.org/10.1093/hmg/ddu390
50. Yokota T, McCourt J, Ma F, Ren S, Li S, Kim TH, *et al.* Type V collagen in scar tissue regulates the size of scar after heart injury. *Cell* 2020;**182**:545–562 e523. https://doi.org/10.1016/j.cell.2020.06.030
51. Arab K, Karaulanov E, Musheev M, Trnka P, Schafer A, Grummt I, *et al.* GADD45A binds R-loops and recruits TET1 to CpG island promoters. *Nat Genet* 2019;**51**:217–223. https://doi.org/10.1038/s41588-018-0306-6
52. Li Z, Gu TP, Weber AR, Shen JZ, Li BZ, Xie ZG, *et al.* Gadd45a promotes DNA demethylation through TDG. *Nucleic Acids Res* 2015;**43**:3986–3997. https://doi.org/10.1093/nar/gkv283
53. Kim JB, Zhao Q, Nguyen T, Pjanic M, Cheng P, Wirka R, *et al.* Environment-sensing aryl hydrocarbon receptor inhibits the chondrogenic fate of modulated smooth muscle cells in atherosclerotic lesions. *Circulation* 2020;**142**:575–590. https://doi.org/10.1161/CIRCULATIONAHA.120.045981
54. Wirka RC, Wagh D, Paik DT, Pjanic M, Nguyen T, Miller CL, *et al.* Atheroprotective roles of smooth muscle cell phenotypic modulation and the TCF21 disease gene as revealed by single-cell analysis. *Nat Med* 2019;**25**:1280–1289. https://doi.org/10.1038/s41591-019-0512-5
55. Querejeta R, Lopez B, Gonzalez A, Sanchez E, Larman M, Martinez Ubago JL, *et al.* Increased collagen type I synthesis in patients with heart failure of hypertensive origin: relation to myocardial fibrosis. *Circulation* 2004;**110**:1263–1268. https://doi.org/10.1161/01.CIR.0000140973.60992.9A
56. Tang J, Su T, Huang K, Dinh PU, Wang Z, Vandergriff A, *et al.* Targeted repair of heart injury by stem cells fused with platelet nanovesicles. *Nat Biomed Eng* 2018;**2**:17–26. https://doi.org/10.1038/s41551-017-0182-x
57. Zhang Y, Zhu D, Wei Y, Wu Y, Cui W, Liuqin L, *et al.* A collagen hydrogel loaded with HDAC7-derived peptide promotes the regeneration of infarcted myocardium with functional improvement in a rodent model. *Acta Biomater* 2019;**86**:223–234. http://dx.doi.org/10.1016/j.actbio.2019.01.022
58. Hou J, Pan Y, Zhu D, Fan Y, Feng G, Wei Y, *et al.* Targeted delivery of nitric oxide via a 'bump-and-hole'-based enzyme–prodrug pair. *Nat Chem Biol* 2019;**15**:151–160. http://dx.doi.org/10.1038/s41589-018-0190-5
59. Maddox TM, Januzzi JL, Allen LA, Breathett K, Butler J, Davis LL, *et al.* 2021 Update to the 2017 ACC Expert Consensus Decision Pathway for Optimization of Heart Failure Treatment: answers to 10 pivotal issues about heart failure with reduced ejection fraction. *J Am Coll Cardiol* 2021;**77**:772–810. doi:10.1016/j.jacc.2020.11.022
60. Fang L, Murphy AJ, Dart AM. A clinical perspective of anti-fibrotic therapies for cardiovascular disease. *Front Pharmacol* 2017;**8**:186. https://doi.org/10.3389/fphar.2017.00186
61. Nagao M, Lyu Q, Zhao Q, Wirka RC, Bagga J, Nguyen T, *et al.* Coronary disease-associated gene TCF21 inhibits smooth muscle cell differentiation by blocking the myocardin-serum response factor pathway. *Circ Res* 2020;**126**:517–529. https://doi.org/10.1161/CIRCRESAHA.119.315968
62. Lu J, Chang P, Richardson JA, Gan L, Weiler H, Olson EN. The basic helix-loop-helix transcription factor capsulin controls spleen organogenesis. *Proc Natl Acad Sci U S A* 2000;**97**:9525–9530. https://doi.org/10.1073/pnas.97.17.9525
63. Shen YC, Shami AN, Moritz L, Larose H, Manske GL, Ma Q, *et al.* TCF21(+) Mesenchymal cells contribute to testis somatic cell development, homeostasis, and regeneration in mice. *Nat Commun* 2021;**12**:3876. https://doi.org/10.1038/s41467-021-24130-8
64. Huang CK, Kafert-Kasting S, Thum T. Preclinical and clinical development of noncoding RNA therapeutics for cardiovascular disease. *Circ Res* 2020;**126**:663–678. https://doi.org/10.1161/CIRCRESAHA.119.315856
65. Barreto G, Schafer A, Marhold J, Stach D, Swaminathan SK, Handa V, *et al.* Gadd45a promotes epigenetic gene activation by repair-mediated DNA demethylation. *Nature* 2007;**445**:671–675. https://doi.org/10.1038/nature05515
66. Kohli RM, Zhang Y. TET enzymes, TDG and the dynamics of DNA demethylation. *Nature* 2013;**502**:472–479. https://doi.org/10.1038/nature12750
67. Aghajanian H, Kimura T, Rurik JG, Hancock AS, Leibowitz MS, Li L, *et al.* Targeting cardiac fibrosis with engineered T cells. *Nature* 2019;**573**:430–433. https://doi.org/10.1038/s41586-019-1546-z
68. Zhao Q, Wirka R, Nguyen T, Nagao M, Cheng P, Miller CL, *et al.* TCF21 and AP-1 interact through epigenetic modifications to regulate coronary artery disease gene expression. *Genome Med* 2019;**11**:23. https://doi.org/10.1186/s13073-019-0635-9
69. Hu B, Lelek S, Spanjaard B, El-Sammak H, Simoes MG, Mintcheva J, *et al.* Origin and function of activated fibroblast states during zebrafish heart regeneration. *Nat Genet* 2022;**54**:1227–1237. https://doi.org/10.1038/s41588-022-01129-5
70. Marro J, Pfefferli C, de Preux Charles AS, Bise T, Jazwinska A. Collagen XII contributes to epicardial and connective tissues in the zebrafish heart during ontogenesis and regeneration. *PLoS One* 2016;**11**:e0165497. https://doi.org/10.1371/journal.pone.0165497